Continuum Mech. Thermodyn. (2023) 35:799–819
https://doi.org/10.1007/s00161-020-00911-2

ORIGINAL ARTICLE

Manuel Ferretti · Francesco D'Annibale · Angelo Luongo

Buckling of tower buildings on elastic foundation under compressive tip forces and self-weight

Received: 6 February 2020 / Accepted: 31 July 2020 / Published online: 18 August 2020

Abstract Buckling of uniformly and not uniformly compressed tower buildings, resting on Winkler type soil, is investigated. An equivalent beam is introduced, able to capture the essential behavior of the building. It is a 3D Timoshenko beam, modeled in the framework of a direct approach, whose constitutive law is derived via a homogenization procedure, which includes the effect of the column prestress. The continuous model is discretized via finite differences, and a linear bifurcation analysis is carried out by solving an algebraic eigenvalue problem. Numerical results are shown for sample problems, aimed at detecting the structural behavior, and illustrating the role of some mechanical parameters. Results supplied by the equivalent beam model are compared with those derived by finite element analyses, carried out on three-dimensional frames.

Keywords Beam-like structures · Equivalent beam model · Timoshenko beam · Homogenization procedure · Buckling analysis

1 Introduction

Buckling analysis of tower buildings is usually carried out through finite element analysis on three-dimensional models, which are typically made of 3D frames and shells elements (see, e.g., [1–3]). This kind of analysis aims to describe the behavior of the building on two different length scales: (i) the local scale of the single structural components; (ii) the global scale of the entire structure. However, it calls for numerical solving of algebraic systems of a large number of degrees of freedom, which is not desirable in a pre-design stage but, instead, has to be performed during the final step of the design process.

On the other end, periodic systems, such as reticulated and pantographic structures [4–10] or multi-storey tower buildings, made of several floors, can be modeled through homogenization procedures. A large number of papers on the topic of homogenization of multi-storey buildings, as beam-like structures, is available in the literature; the reader is referred to some of them [11–21]. In this context, an equivalent continuous model, able to capture the essential behavior of the structure, is desirable at the pre-design stage, as well as for assessment of existing buildings, due to its reduced number of the degrees of freedom and simplicity. But, as counterpart, an homogenized model is able to retain information only on the global scale of the structure, thus being not suitable to describe local buckling phenomena, which, instead, occurs on the length scale of the floor.

Communicated by Luca Placidi.

M. Ferretti · F. D'Annibale (✉) · A. Luongo
Department of Civil, Construction-Architectural and Environmental Engineering, University of L'Aquila, 67100 L'Aquila, Italy
E-mail: francesco.dannibale@univaq.it

M. Ferretti · F. D'Annibale · A. Luongo
International Research Center on Mathematics and Mechanics of Complex Systems, University of L'Aquila, 67100 L'Aquila, Italy

Some interesting works of literature have been focused on reduced continuous models for buckling analysis of tower buildings [18,22–24]. Among them, in [22,23] an heuristic approach is proposed for the analysis of flexural–torsional buckling of multi-store buildings under self-weight. In [18] an equivalent sandwich beam model is defined for the modal and buckling analyses of buildings. In [24] a Timoshenko beam model, embedded in a 3D space, is introduced for buckling analysis of multi-storey buildings, made by rigid floors connected by elastic columns, via a suitable homogenization procedure. There, a bifurcation analysis for the case of uniformly compressed buildings is addressed, and numerical comparisons between the Timoshenko model and finite element analyses on 3D-frames are carried out, showing the effectiveness of the former model in describing the relevant behavior of the building.

The present work is an extension of what has been done in [24]. The aim is to analyze the flexural–torsional buckling behavior of tower buildings, in the presence of both distributed gravitational loads (representative of self-weight), and tip (point) forces, applied at the top floor. Moreover, the interaction with a soil, modeled as Winkler elastic springs, is also studied, and its effects on the global buckling of the buildings are evaluated. To this end, an equivalent 3D Timoshenko beam model is formulated in the framework of a direct approach, whose constitutive law is derived through a homogenization procedure (see, e.g., [25–30]). The developed up-scaling method couples the *heuristic approaches*, which a priori define the equivalent model but do not relates the micro- and macro-descriptions, and the *asymptotic homogenization method*, in which the effective model is derived and the micro- and macro-relations are defined. Indeed, in the present paper, the effective model, i.e., a Timoshenko beam embedded in a 3D-space, is a priori assumed, and, in conjunction, the tools of the homogenization are used to explicitly get analytical micro-/macro-relationships in its constitutive law. The treatment is similar to that followed in [15–17,31], but here the effects of the prestress forces in the columns are accounted for, thus introducing a geometric effect in the elastic law. All the results, given by the equivalent continuous model, are compared with those obtained through finite-element analyses carried out on three-dimensional frames.

The paper is organized as follows. In Sect. 2 the equivalent Timoshenko beam model is formulated. In Sect. 3 the bifurcation problem is posed, bifurcation parameters are introduced, and a numerical discretization scheme is defined. In Sect. 4 numerical results, concerning both symmetric and not symmetric buildings, are presented and discussed. In Sect. 5 some conclusions are drawn. Two appendices, giving details on soil modeling and on the definition of some linear differential operators, close the paper.

2 Model

A tower building is considered, made of an assembly of equal rigid floors connected by elastic columns, i.e., a *periodic* beam-like structure, as shown in Fig. 1a. The structure has vertical axis $\bar{\mathbf{a}}_x$, and it is subjected

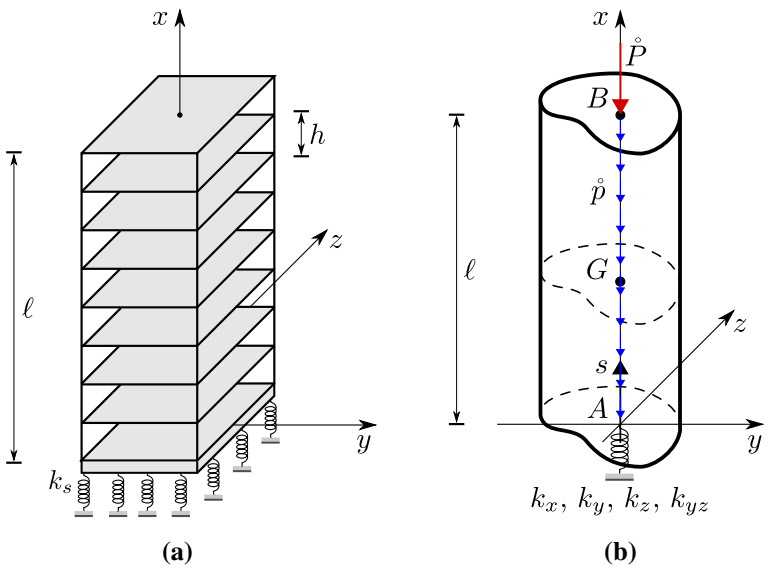

Fig. 1 Multi-store building on elastic foundation (**a**) and equivalent Timoshenko beam (**b**)

to: (i) a centroidal compressive force $\mathbf{F} = -F\bar{\mathbf{a}}_x$ acting at the top floor n and, (ii) equal gravitational loads $\mathbf{W}_j = -W\bar{\mathbf{a}}_x$ applied at the floors $j = 1, 2, \ldots n$. Goal of the analysis is to find the combinations of F and W (taken as scalar *independent* bifurcation parameters), which trigger static bifurcation (buckling) of the structure.

The discrete system (*fine model*) is modeled, via a continuization procedure, as an equivalent *3D-Timoshenko beam* (*rough model*), i.e., as an internally unconstrained 1D polar continuum, whose particles posses 6 degree-of-freedom, three translations and three rotations, as shown in Fig. 1b. The beam axis $\bar{\mathbf{a}}_x$ is taken coincident with the axis which contains the (geometrical) centroids of the floors, although generally this is not the axis of the elastic centers; two principal inertia axes, $\bar{\mathbf{a}}_y, \bar{\mathbf{a}}_z$, complete the orthogonal basis. The continuous model is endowed with a suitable elastic law which is determined via an energy equivalence between the fine and rough model [17,24].

The beam is assumed to be free at the top end B and elastically restrained at the lower end A by an extensional spring of stiffness k_x and by rotational springs of stiffnesses k_y, k_z, k_{yz}. This system of springs must be meant as equivalent to a homogeneous Winkler soil, applying vertical elastic forces to a rigid foundation. The expressions of the constants are defined in the Appendix A.

Elastic versus rigid soils

A preliminary discussion on the effects of the soil elasticity on the mechanical behavior of the tower building is addressed. This is carried out via an order-of-magnitude analysis of the equivalent system elastic energy, when (i) the beam is clamped or (ii) it is elastically restrained by a rotational spring. A uniformly distributed horizontal load is considered, of linear density p, acting in the $\bar{\mathbf{a}}_y$-direction without eccentricity with respect the centroidal vertical axis x.

Bending moment and shear force at the abscissa s read:

$$\begin{aligned} T_y(s) &= p(\ell - s), \\ M_z(s) &= \frac{1}{2} p(\ell - s)^2. \end{aligned} \tag{1}$$

The corresponding complementary elastic energies, U_c and U_{el}, which are referred to clamped and elastically restrained beams, respectively, are:

$$\begin{aligned} U_c &= \frac{1}{2}\int_0^\ell \left(\frac{T_y^2}{GA} + \frac{M_z^2}{EI}\right) \mathrm{d}s = \frac{1}{2}\left(\frac{p^2\ell^3}{3GA} + \frac{p^2\ell^5}{20EI}\right), \\ U_{el} &= \frac{1}{2}\int_0^\ell \left(\frac{T_y^2}{GA} + \frac{M_z^2}{EI}\right) \mathrm{d}s + \frac{1}{2}\frac{M_{zA}^2}{k} = \frac{1}{2}\left(\frac{p^2\ell^3}{3GA} + \frac{p^2\ell^5}{20EI} + \frac{p^2\ell^4}{4k}\right), \end{aligned} \tag{2}$$

where $M_{zA} := M_z(0)$, and, moreover, GA, EI are the shear and bending stiffnesses of the equivalent column, k is the stiffness of the rotational spring, respectively.

The energy ratio $r := U_{el}/U_c$ reads:

$$r = 1 + \frac{15\,EI\,GA\,\ell}{k\left(20\,EI + 3\,GA\,\ell^2\right)} = 1 + \mathcal{O}\left(\frac{EI}{k\ell}\right), \tag{3}$$

where, in the second equality, $GA\ell^2 = \mathcal{O}(EI)$ has been taken, meaning that the shear strain is not negligible. Moreover, for a building having a square floor of side b, equal columns of height h and axial stiffness EA_c, it is (see Appendices A and B) $EI = \mathcal{O}\left(EA_c b^2\right)$, $k = \mathcal{O}\left(k_s b^4\right)$, k_s being the soil elastic constant. Therefore:

$$r = 1 + \mathcal{O}\left(\frac{EA_c}{k_s b^2 \ell}\right) = 1 + \mathcal{O}\left(\frac{E}{k_s h}\,\frac{A_c}{b^2}\,\frac{h}{\ell}\right). \tag{4}$$

In real applications, the ratio $E/(k_s h) = \mathcal{O}\left(10^4\right)$, when the soil is soft and steel columns are considered, and $A_c/b^2 = \mathcal{O}\left(10^{-4}\right)$. Since $\ell = n\,h$, it follows:

$$r = 1 + \mathcal{O}\left(\frac{1}{n}\right). \tag{5}$$

It is concluded that, the differences between the energies of an elastically restrained and of a clamped beam can be significant only when n is small. In other words, when tall buildings are considered, $r \to 1$ and $U_{el} \to U_c$, i.e., the soil can be modeled as rigid. Numerical results, presented in the following sections, shed light on these aspects, also on a quantitative side.

Precritical state

The Timoshenko beam is referred to a material abscissa $s \in [0, \ell]$, $\ell := n\,h$ being the total beam length and h the inter-floor height. By uniformly spreading the point loads W on the inter-floor, the following forces are considered for the equivalent beam:

- uniformly distributed forces $\mathbf{p}(s) = -\mathring{p}\,\bar{\mathbf{a}}_x$, in the field $[0, \ell]$, with $\mathring{p} = \frac{W}{h} = \text{const}$;
- a force $\mathbf{P} = -\mathring{P}\,\bar{\mathbf{a}}_x$, applied at the tip B, with $\mathring{P} := F + \frac{1}{2}W$.

All these forces are applied to the beam axis $\bar{\mathbf{a}}_x$, and therefore they induce a (linearly variable) compressive stress:

$$\mathring{N}(s) := -\mathring{P} - \mathring{p}\,(\ell - s)\,. \tag{6}$$

Due the eccentricity of the elastic center with respect the centroid, the beam undergoes bending, in addition to extension in the precritical state. However, as customary in linear bifurcation analysis, any precritical strain is neglected, so that the configuration of the beam at the bifurcation is confused with the straight and unstretched natural configuration.

Kinematics

The configuration variables of the beam are the displacement vector $\mathbf{u} = u(s)\,\bar{\mathbf{a}}_x + v(s)\,\bar{\mathbf{a}}_y + w(s)\,\bar{\mathbf{a}}_z$ and the rotation tensor $\mathbf{R}(s)$. This latter leads the *reference basis* $\bar{\mathcal{B}} := \left(\bar{\mathbf{a}}_x, \bar{\mathbf{a}}_y, \bar{\mathbf{a}}_z\right)$, attached to the cross section, to the *current basis* $\mathcal{B}(s) := \left(\mathbf{a}_x(s), \mathbf{a}_y(s), \mathbf{a}_z(s)\right) = \mathbf{R}(s)\left(\bar{\mathbf{a}}_x, \bar{\mathbf{a}}_y, \bar{\mathbf{a}}_z\right)$. Its representation on $\bar{\mathcal{B}}$ is:

$$\boldsymbol{R} = \begin{bmatrix} \cos\left(\theta_y\right)\cos\left(\theta_z\right) & \sin\left(\theta_x\right)\sin\left(\theta_y\right)\cos\left(\theta_z\right) & \cos\left(\theta_x\right)\sin\left(\theta_y\right)\cos\left(\theta_z\right) \\ & -\cos\left(\theta_x\right)\sin\left(\theta_z\right) & +\sin\left(\theta_x\right)\sin\left(\theta_z\right) \\ \cos\left(\theta_y\right)\sin\left(\theta_z\right) & \sin\left(\theta_x\right)\sin\left(\theta_y\right)\sin\left(\theta_z\right) & \cos\left(\theta_x\right)\sin\left(\theta_y\right)\sin\left(\theta_z\right) \\ & +\cos\left(\theta_x\right)\cos\left(\theta_z\right) & -\sin\left(\theta_x\right)\cos\left(\theta_z\right) \\ -\sin\left(\theta_y\right) & \sin\left(\theta_x\right)\cos\left(\theta_y\right) & \cos\left(\theta_x\right)\cos\left(\theta_y\right) \end{bmatrix}, \tag{7}$$

where $\theta_x, \theta_y, \theta_z$ are three elementary rotations of the cross section (see, e.g., [5]); the dependency on s of the rotation angles is omitted for the sake of brevity. By linearizing kinematics around the trivial configuration, it follows:

$$\boldsymbol{R} \simeq \begin{bmatrix} 1 & -\theta_z & \theta_y \\ \theta_z & 1 & -\theta_x \\ -\theta_y & \theta_x & 1 \end{bmatrix}. \tag{8}$$

The following exact strain–displacement relationships are adopted [5,32–36]:

$$\begin{aligned} \mathbf{e} &:= \mathbf{R}^T\left(\bar{\mathbf{a}}_x + \mathbf{u}'\right) - \bar{\mathbf{a}}_x, \\ \mathbf{k} &:= \text{axial}\left[\mathbf{R}^T\mathbf{R}'\right], \end{aligned} \tag{9}$$

where $\mathbf{e} = \varepsilon(s)\,\bar{\mathbf{a}}_x + \gamma_y(s)\,\bar{\mathbf{a}}_y + \gamma_z(s)\,\bar{\mathbf{a}}_z$ is the strain vector, $\mathbf{k} = \kappa_x(s)\,\bar{\mathbf{a}}_x + \kappa_y(s)\,\bar{\mathbf{a}}_y + \kappa_z(s)\,\bar{\mathbf{a}}_z$ the curvature vector and a dash denotes differentiation with respect to s. By linearizing the strains, it follows:

$$\begin{aligned} \varepsilon &= u', \\ \gamma_y &= v' - \theta_z, \\ \gamma_z &= w' + \theta_y, \\ \kappa_x &= \theta_x', \\ \kappa_y &= \theta_y', \\ \kappa_z &= \theta_z'. \end{aligned} \tag{10}$$

The (geometric) boundary conditions at the lower end A require:

$$v_A = w_A = \theta_{xA} = 0. \tag{11}$$

Balance equations

The exact balance equations for the beam (with no couples applied) are:

$$\begin{aligned} &\mathbf{t}' + \mathbf{p} = \mathbf{0}, \\ &\mathbf{m}' + \left(\bar{\mathbf{a}}_x + \mathbf{u}'\right) \times \mathbf{t} = \mathbf{0}, \end{aligned} \tag{12}$$

where $\mathbf{t} = N(s)\,\bar{\mathbf{a}}_x + T_y(s)\,\bar{\mathbf{a}}_y + T_z(s)\,\bar{\mathbf{a}}_z$ is the stress-force, $\mathbf{m} = M_x(s)\,\bar{\mathbf{a}}_x + M_x(s)\,\bar{\mathbf{a}}_y + M_z(s)\,\bar{\mathbf{a}}_z$ the stress-couple and $\mathbf{p} := -\mathring{p}(s)\,\bar{\mathbf{a}}_x$ the external distributed force. By projecting these equations onto the current basis, it follows:

$$\begin{aligned} &N' - \kappa_z T_y + \kappa_y T_z + p_x = 0, \\ &T_y' + \kappa_z N - \kappa_x T_z + p_y = 0, \\ &T_z' - \kappa_y N + \kappa_x T_y + p_z = 0, \\ &M_x' - \kappa_z M_y + \kappa_y M_z - \gamma_z T_y + \gamma_y T_z = 0, \\ &M_y' + \kappa_z M_x - \kappa_x M_z + \gamma_z N - (1+\varepsilon)\,T_z = 0, \\ &M_z' - \kappa_y M_x + \kappa_x M_y - \gamma_y N + (1+\varepsilon)\,T_y = 0, \end{aligned} \tag{13}$$

where $p_\alpha = \mathbf{p}\cdot\mathbf{a}_\alpha = -\mathring{p}\,\bar{\mathbf{a}}_x \cdot \mathbf{R}\bar{\mathbf{a}}_\alpha$ $(\alpha = x, y, z)$ are the components of $\mathbf{p}$ in $\mathcal{B}$. Using the linear approximation for $\mathbf{R}$ (i.e., Eq (8)), it is $p_x \simeq -\mathring{p}$, $p_y \simeq \mathring{p}\,\theta_z$, $p_z \simeq -\mathring{p}\,\theta_y$.

To obtain incremental balance equations, the stresses are expressed as:

$$N = \mathring{N} + \tilde{N}, \qquad T_y = \tilde{T}_y, \qquad T_z = \tilde{T}_z, \qquad M_x = \tilde{M}_x, \qquad M_y = \tilde{M}_y, \qquad M_z = \tilde{M}_z, \tag{14}$$

in which $\mathring{N}$ is the (known) prestress and the tilde denotes an incremental quantity. By substituting these positions in Eq (13), accounting for the precritical equilibrium $\mathring{N}' - \mathring{p} = 0$ and the linear strain–displacement relationships (10), and finally linearizing in the incremental quantities, the following equations are obtained:

$$\begin{aligned} &\tilde{N}' = 0, \\ &\tilde{T}_y' + \left(\mathring{N}\theta_z\right)' = 0, \\ &\tilde{T}_z' - \left(\mathring{N}\theta_y\right)' = 0, \\ &\tilde{M}_x' = 0, \\ &\tilde{M}_y' + \mathring{N}\left(w' + \theta_y\right) - \tilde{T}_z = 0, \\ &\tilde{M}_z' - \mathring{N}\left(v' - \theta_z\right) + \tilde{T}_y = 0, \end{aligned} \tag{15}$$

At the free end B a force $\mathbf{P} = -\mathring{P}\,\bar{\mathbf{a}}_x$ is applied; the boundary conditions therefore are: $\mathbf{t}_B = \mathbf{P}$, $\mathbf{m}_B = \mathbf{0}$. By projecting onto the current basis:

$$\begin{aligned} &N_B = P_x, \quad &&T_{yB} = P_y, \quad &&T_{zB} = P_z, \\ &M_{xB} = 0, \quad &&M_{yB} = 0, \quad &&M_{zB} = 0, \end{aligned} \tag{16}$$

where $P_\alpha = \mathbf{P}\cdot\mathbf{a}_\alpha = -\mathring{P}\,\bar{\mathbf{a}}_x \cdot \mathbf{R}\bar{\mathbf{a}}_\alpha$ $(\alpha = x, y, z)$ are the components of $\mathbf{P}$ in $\mathcal{B}(\ell)$. By using linear kinematics, the boundary condition in the precritical state $\mathring{N}(\ell) = -\mathring{P}$, and linearizing in the incremental quantities, the boundary conditions at B become:

$$\begin{aligned} &\tilde{N}_B = 0, \quad &&\tilde{T}_{yB} = \mathring{P}\theta_{zB}, \quad &&\tilde{T}_{zB} = -\mathring{P}\theta_{yB}, \\ &\tilde{M}_{xB} = 0, \quad &&\tilde{M}_{yB} = 0, \quad &&\tilde{M}_{zB} = 0. \end{aligned} \tag{17}$$

Equilibrium at the lower end A requires $-\mathbf{t}_A = \mathbf{F}^{el}$, $-\mathbf{m}_A = \mathbf{C}^{el}$, with $\mathbf{F}^{el}$, $\mathbf{C}^{el}$ the foundation elastic reactions. By using linear kinematics for the rotations, it is $\mathbf{F}^{el} = -k_x u_A \bar{\mathbf{a}}_x$, $\mathbf{C}^{el} = \left(-k_y\theta_{yA} + k_{yz}\theta_{zA}\right)\bar{\mathbf{a}}_y + \left(-k_z\theta_{zA} + k_{yz}\theta_{yA}\right)\bar{\mathbf{a}}_z$, see the Appendix A. Projection onto the current basis leads to:

$$-N_A = F_x^{el}, \qquad -M_{yA} = C_y^{el}, \qquad -M_{zA} = C_z^{el}, \tag{18}$$

where, at first order, $F_x^{el} \simeq -k_x u_A$, $C_y^{el} \simeq -k_y\theta_{yA} + k_{yz}\theta_{zA}$, $C_z^{el} \simeq -k_z\theta_{zA} + k_{yz}\theta_{yA}$. In incremental form, the boundary conditions read:

$$\tilde{N}_A = k_x u_A, \qquad \tilde{M}_{yA} = k_y\theta_{yA} - k_{yz}\theta_{zA}, \qquad \tilde{M}_{zA} = k_z\theta_{zA} - k_{yz}\theta_{yA}, \tag{19}$$

in which u_A should be meant as the incremental displacement with respect the precritical displacement, namely $\mathring{u}_A = \mathring{N}_A/k_x$ that is not taken into account in the present analysis. When the soil is rigid (i.e., k_x, k_y, k_z, k_{yz} tend to infinity), then Eq. (19) must be replaced by $u_A = \theta_{yA} = \theta_{zA} = 0$.

A virtual work approach

It is worth noticing that the equilibrium problem (15), (17) and (19) can alternatively be derived by the virtual work principle, directly expressed in terms of incremental quantities, namely:

$$\begin{aligned} &\int_0^\ell \left(\tilde{N}\delta\varepsilon + \tilde{T}_y\delta\gamma_y + \tilde{T}_z\delta\gamma_z + \tilde{M}_x\delta\kappa_x + \tilde{M}_y\delta\kappa_y + \tilde{M}_z\delta\kappa_z\right)\mathrm{d}s + \int_0^\ell \mathring{N}\delta\varepsilon^{(2)}\mathrm{d}s \\ &+ k_x u_A\delta u_A + \left(k_y\theta_{yA} - k_{yz}\theta_{zA}\right)\delta\theta_{yA} + \left(k_z\theta_{zA} - k_{yz}\theta_{yA}\right)\delta\theta_{zA} = 0, \qquad \forall\left(\delta u, \delta v, \delta w, \delta\theta_x, \delta\theta_y, \delta\theta_z\right), \end{aligned} \tag{20}$$

in which the first integral represents the internal virtual work of the incremental stresses, the second integral the second-order virtual work of the prestress, and the boundary terms the virtual work of the soil elastic reactions. Here, $\delta\varepsilon, \delta\gamma_y, \ldots, \delta\kappa_z$ are related to $\delta u, \delta v, \ldots, \delta\theta_z$ via the linear strain–displacement relationships (10), while $\delta\varepsilon^{(2)}$ is the first variation of the second-order part of the exact unit-extension $\varepsilon := \bar{\mathbf{a}}_x \cdot \left(\mathbf{R}^T\left(\bar{\mathbf{a}}_x + \mathbf{u}'\right) - \bar{\mathbf{a}}_x\right)$; when this is Taylor-expanded, it reads:

$$\varepsilon^{(2)} := -\frac{1}{2}\left(\theta_y^2 + \theta_z^2\right) + \theta_z v' - \theta_y w'. \tag{21}$$

By performing standard steps of variational calculus and accounting for the geometric boundary conditions (11), the equilibrium equations and mechanical boundary conditions are recovered.

Elastic law

A linear hyper-elastic law is assumed, linking incremental stresses to strains, in which, however, the elastic constants depend on the prestress, namely:

$$\tilde{\boldsymbol{\sigma}} = \boldsymbol{C}\left(\mathring{N}\right)\boldsymbol{\varepsilon}, \tag{22}$$

where $\tilde{\boldsymbol{\sigma}} := \left(\tilde{N},\ \tilde{T}_y,\ \tilde{T}_z,\ \tilde{M}_x,\ \tilde{M}_y,\ \tilde{M}_z\right)^T$ and $\boldsymbol{\varepsilon} := \left(\varepsilon,\ \gamma_y,\ \gamma_z,\ \kappa_x,\ \kappa_y,\ \kappa_z\right)^T$. Since $\mathring{N}$ is small with respect the axial stiffness, the elastic matrix can be expanded in series, as $\boldsymbol{C}\left(\mathring{N}\right) = \boldsymbol{C}\,(0) + \frac{\partial \boldsymbol{C}(0)}{\partial \mathring{N}}\mathring{N} + \ldots$, and the series truncated at first order. Therefore:

$$\tilde{\boldsymbol{\sigma}} = \left(\boldsymbol{C}^0 + \mathring{N}\,\hat{\boldsymbol{C}}\right)\boldsymbol{\varepsilon}, \tag{23}$$

in which $\boldsymbol{C}^0$ is the elastic matrix at the natural state, and $\hat{\boldsymbol{C}}$ its first derivative at the origin with respect the prestress.

It is important to remark that the geometric effects, induced by the precritical stresses, affect the equivalent model both in the equilibrium equations (15) and (17), and in the constitutive law (23). While the former contribution is expected, since always appears in classical buckling problems, the latter is not common from a modeling point of view, and its effects deserve to be explored. Similar circumstance occurs in the classical model of the compressed Vlasov thin-walled beam; there, the geometric torsional stiffness emerges from a 3D fiber micro-model, which has necessarily to be included in the constitutive law, when a direct 1D model is formulated.

Identification of the elastic constants

The task is now how to identify the coefficients of the two 6×6 symmetric elastic matrices $\boldsymbol{C}^0$, $\hat{\boldsymbol{C}}$, in order for the rough model captures at the best extent the mechanical behavior of the fine model. The problem has been addressed in [17] for non-prestressed buildings, and in [24] for uniformly compressed buildings. The results of this latter paper can be directly applied to the problem at hand, due to the fact the self-weight of the building is applied just at the floors, so that the prestress of columns is *stepwise constant*. The procedure is, therefore, only sketched here, while the reader is referred to [24] for additional details.

The identification of the elastic constants is based on a continuization procedure which preserves the elastic energy. It is carried out via the following steps.

1. A segment of beam of length h, equal to the interfloor height, is considered to undergo an uniform state of strain $\boldsymbol{\varepsilon}$; consistently with the assumed constitutive law (23), the elastic energy of the rough model is:

$$U_r = h\frac{1}{2}\boldsymbol{\varepsilon}^T\left(\boldsymbol{C}^0 + \mathring{N}\hat{\boldsymbol{C}}\right)\boldsymbol{\varepsilon}. \tag{24}$$

2. The relative displacements of the two cross sections bounding the segment are found by integration of the linear strain–displacement relationships (10), i.e.,

$$\begin{pmatrix} u_G \\ v_G \\ w_G \\ \theta_x \\ \theta_y \\ \theta_z \end{pmatrix} = \begin{bmatrix} h & 0 & 0 & 0 & 0 & 0 \\ 0 & h & 0 & 0 & 0 & \frac{h^2}{2} \\ 0 & 0 & h & 0 & -\frac{h^2}{2} & 0 \\ 0 & 0 & 0 & h & 0 & 0 \\ 0 & 0 & 0 & 0 & h & 0 \\ 0 & 0 & 0 & 0 & 0 & h \end{bmatrix} \begin{pmatrix} \varepsilon \\ \gamma_y \\ \gamma_z \\ \kappa_x \\ \kappa_y \\ \kappa_z \end{pmatrix} \quad \text{or} \quad \boldsymbol{u}_G = \boldsymbol{B}\boldsymbol{\varepsilon}, \tag{25}$$

where an index G remembers that translations are referred to the centroid.

3. Such displacements are assigned to the upper floor of a cell of the fine model, made of two adjacent floors connected by N elastic columns, modeled as microscopic Timoshenko beams, whose principal inertia axes are aligned with the basis $\bar{\mathcal{B}}$. The elastic energy stored by the fine model, is evaluated as:

$$U_f = \sum_{i=1}^{N} \frac{1}{2} \boldsymbol{u}_i^T \left(\boldsymbol{K}_i^0 + \mathring{N}_i \hat{\boldsymbol{K}}_i \right) \boldsymbol{u}_i, \tag{26}$$

where: $\boldsymbol{u}_i$ are the six displacements of the head of the i-th column, related to the displacements (25) by linear kinematic relationships:

$$\begin{pmatrix} u_i \\ v_i \\ w_i \\ \theta_{xi} \\ \theta_{yi} \\ \theta_{zi} \end{pmatrix} = \begin{bmatrix} 1 & 0 & 0 & 0 & z_i & -y_i \\ 0 & 1 & 0 & -z_i & 0 & 0 \\ 0 & 0 & 1 & y_i & 0 & 0 \\ 0 & 0 & 0 & 1 & 0 & 0 \\ 0 & 0 & 0 & 0 & 1 & 0 \\ 0 & 0 & 0 & 0 & 0 & 1 \end{bmatrix} \begin{pmatrix} u_G \\ v_G \\ w_G \\ \theta_x \\ \theta_y \\ \theta_z \end{pmatrix} \quad \text{or} \quad \boldsymbol{u}_i = \boldsymbol{A}_i \boldsymbol{u}_G, \tag{27}$$

in which y_i, z_i are the coordinates of the head of the column; $\mathring{N}_i := \eta_i \mathring{N}$ is the prestress of the i-th column (with η_i a nondimensional quota), determined by ignoring small bending moments, which are due to the eccentricity existing between the centroid of the floor and the elastic center of the columns; $\boldsymbol{K}_i^0$ is the elastic stiffness matrix of the i-th column, and $\hat{\boldsymbol{K}}_i$ is its geometric stiffness matrix. By using Eqs. (25) and (27), it is also:

$$U_f = \boldsymbol{B}^T \left(\sum_{i=1}^{N} \frac{1}{2} \boldsymbol{A}_i^T \left(\boldsymbol{K}_i^0 + \eta_i \mathring{N} \hat{\boldsymbol{K}}_i \right) \boldsymbol{A}_i \right) \boldsymbol{B} \boldsymbol{\varepsilon}. \tag{28}$$

4. By requiring that the two energies, (24) and (28), are equal for any $\boldsymbol{\varepsilon}$, the desired elastic matrices for the rough model are finally found:

$$\boldsymbol{C}^0 = \frac{1}{h} \boldsymbol{B}^T \left(\sum_{i=1}^{N} \boldsymbol{A}_i^T \boldsymbol{K}_i^0 \boldsymbol{A}_i \right) \boldsymbol{B}, \qquad \hat{\boldsymbol{C}} = \frac{1}{h} \boldsymbol{B}^T \left(\sum_{i=1}^{N} \eta_i \boldsymbol{A}_i^T \hat{\boldsymbol{K}}_i \boldsymbol{A}_i \right) \boldsymbol{B}. \tag{29}$$

Their explicit expressions are reported in the Appendix B.

It should be remarked from the procedure illustrated, that the dependence on prestress of the constitutive law for the macro-beam is captured by accounting for the geometric effects affecting the micro-beams.

The cell critical load

Since the elastic matrix $\boldsymbol{C}\left(\mathring{N}\right) := \boldsymbol{C}^0 + \mathring{N} \hat{\boldsymbol{C}}$ depends on prestress, it can become singular for some $\mathring{N}$. The occurrence of this situation entails buckling of the single cell. The smallest value of the compressive force $P = -\mathring{N}$ which causes the phenomenon will be referred to as the *cell critical load* $P_c^\star$. It is the smallest root of the algebraic equation:

$$\det \left[\boldsymbol{C}^0 - P_c^\star \hat{\boldsymbol{C}} \right] = 0. \tag{30}$$

3 The bifurcation problem

The bifurcation problem is now recast in matrix form, and strategy solutions discussed.

Matrix formulation

The elastic problem is governed by the field equations (10), (15) and (23), with the boundary conditions (11), (19) and (17). They can be rewritten in matrix form, both in the field:

$$\begin{aligned}
&\boldsymbol{\varepsilon} = \boldsymbol{u}' + \boldsymbol{\Gamma}\boldsymbol{u},\\
&\tilde{\boldsymbol{\sigma}}' - \boldsymbol{\Gamma}^T\tilde{\boldsymbol{\sigma}} - \left(\mathring{N}\boldsymbol{\Gamma}\boldsymbol{u}\right)' + \mathring{N}\left(\boldsymbol{\Gamma}^T\boldsymbol{u}' + \boldsymbol{\Omega}\boldsymbol{u}\right) = \boldsymbol{0},\\
&\tilde{\boldsymbol{\sigma}} = \left(\boldsymbol{C}^0 + \mathring{N}\hat{\boldsymbol{C}}\right)\boldsymbol{\varepsilon},
\end{aligned} \tag{31}$$

and at the boundary:

$$\begin{aligned}
\boldsymbol{A}_u\boldsymbol{u}_A &= \boldsymbol{0},\\
\boldsymbol{A}_\sigma\tilde{\boldsymbol{\sigma}}_A &= \boldsymbol{K}_s\boldsymbol{A}_\sigma\boldsymbol{u}_A,\\
\tilde{\boldsymbol{\sigma}}_B &= \mathring{N}_B\boldsymbol{\Gamma}\boldsymbol{u}_B.
\end{aligned} \tag{32}$$

Here: $\boldsymbol{u} := \left(u, v, w, \theta_x, \theta_y, \theta_z\right)^T$ is the displacement column vector; $\boldsymbol{\Gamma}$, $\boldsymbol{\Omega}$, as $\boldsymbol{A}_u$, $\boldsymbol{A}_\sigma$, are Boolean matrices:

$$\boldsymbol{\Gamma} := \begin{bmatrix} 0&0&0&0&0&0\\ 0&0&0&0&0&-1\\ 0&0&0&0&1&0\\ 0&0&0&0&0&0\\ 0&0&0&0&0&0\\ 0&0&0&0&0&0 \end{bmatrix}, \qquad \boldsymbol{\Omega} := \begin{bmatrix} 0&0&0&0&0&0\\ 0&0&0&0&0&0\\ 0&0&0&0&0&0\\ 0&0&0&0&0&0\\ 0&0&0&0&1&0\\ 0&0&0&0&0&1 \end{bmatrix},$$

$$\boldsymbol{A}_u := \begin{bmatrix} 0&1&0&0&0&0\\ 0&0&1&0&0&0\\ 0&0&0&1&0&0 \end{bmatrix}, \qquad \boldsymbol{A}_\sigma := \begin{bmatrix} 1&0&0&0&0&0\\ 0&0&0&0&1&0\\ 0&0&0&0&0&1 \end{bmatrix}, \tag{33}$$

and $\boldsymbol{K}_s$ is the soil stiffness matrix:

$$\boldsymbol{K}_s := \begin{bmatrix} k_x & 0 & 0\\ 0 & k_y & -k_{yz}\\ 0 & -k_{yz} & k_z \end{bmatrix}. \tag{34}$$

By expressing equilibrium in terms of displacements, the elastic problem is governed by the following set of ordinary differential equations:

$$\boldsymbol{D}_2\left(\mathring{N}\right)\boldsymbol{u}'' + \boldsymbol{D}_1\left(\mathring{N}, \mathring{N}'\right)\boldsymbol{u}' + \boldsymbol{D}_0\left(\mathring{N}, \mathring{N}'\right)\boldsymbol{u} = \boldsymbol{0}, \tag{35}$$

with the boundary conditions:

$$\begin{aligned}
&\boldsymbol{A}_u\boldsymbol{u}_A = \boldsymbol{0},\\
&\boldsymbol{B}_{H1}\left(\mathring{N}_H\right)\boldsymbol{u}'_H + \boldsymbol{B}_{H0}\left(\mathring{N}_H\right)\boldsymbol{u}_H = \boldsymbol{0}, \qquad H = A, B.
\end{aligned} \tag{36}$$

In the previous equations, matrices $\boldsymbol{D}$ and $\boldsymbol{B}$ linearly depend on prestress and, possibly, on its gradient, according to:

$$\begin{aligned}
\boldsymbol{D}_2\left(\mathring{N}\right) &:= \boldsymbol{D}_2^0 + \mathring{N}\hat{\boldsymbol{D}}_2,\\
\boldsymbol{D}_i\left(\mathring{N}, \mathring{N}'\right) &:= \boldsymbol{D}_i^0 + \mathring{N}\hat{\boldsymbol{D}}_i + \mathring{N}'\check{\boldsymbol{D}}_i, \quad i = 0, 1,\\
\boldsymbol{B}_{Hj}\left(\mathring{N}_H\right) &:= \boldsymbol{B}_{Hj}^0 + \mathring{N}_H\hat{\boldsymbol{B}}_{Hj}, \qquad j = 0, 1, \quad H = A, B,
\end{aligned} \tag{37}$$

where the following positions hold, in the field:

$$\begin{aligned}
&\boldsymbol{D}_2^0 := \boldsymbol{C}^0, && \hat{\boldsymbol{D}}_2 := \hat{\boldsymbol{C}}, && \\
&\boldsymbol{D}_1^0 := \boldsymbol{C}^0\boldsymbol{\Gamma} - \boldsymbol{\Gamma}^T\boldsymbol{C}^0, && \hat{\boldsymbol{D}}_1 := \hat{\boldsymbol{C}}\boldsymbol{\Gamma} - \boldsymbol{\Gamma}^T\hat{\boldsymbol{C}} + \boldsymbol{\Gamma}^T - \boldsymbol{\Gamma}, && \check{\boldsymbol{D}}_1 := \hat{\boldsymbol{C}}, \\
&\boldsymbol{D}_0^0 := -\boldsymbol{\Gamma}^T\boldsymbol{C}^0\boldsymbol{\Gamma}, && \hat{\boldsymbol{D}}_0 := -\boldsymbol{\Gamma}^T\hat{\boldsymbol{C}}\boldsymbol{\Gamma} + \boldsymbol{\Omega}, && \check{\boldsymbol{D}}_0 := \hat{\boldsymbol{C}}\boldsymbol{\Gamma} - \boldsymbol{\Gamma},
\end{aligned} \tag{38}$$

and at the boundary:

$$\begin{aligned}
&\boldsymbol{B}_{A1}^0 := \boldsymbol{A}_{\boldsymbol{\sigma}}\boldsymbol{C}^0, && \hat{\boldsymbol{B}}_{A1} := \boldsymbol{A}_{\boldsymbol{\sigma}}\hat{\boldsymbol{C}}, \\
&\boldsymbol{B}_{A0}^0 := \boldsymbol{A}_{\boldsymbol{\sigma}}\boldsymbol{C}^0\boldsymbol{\Gamma} - \boldsymbol{K}_s\boldsymbol{A}_{\sigma}, && \hat{\boldsymbol{B}}_{A0} := \boldsymbol{A}_{\boldsymbol{\sigma}}\hat{\boldsymbol{C}}\boldsymbol{\Gamma}, \\
&\boldsymbol{B}_{B1}^0 := \boldsymbol{C}^0, && \hat{\boldsymbol{B}}_{B1} := \hat{\boldsymbol{C}}, \\
&\boldsymbol{B}_{B0}^0 := \boldsymbol{C}^0\boldsymbol{\Gamma}, && \hat{\boldsymbol{B}}_{B0} := \hat{\boldsymbol{C}}\boldsymbol{\Gamma} - \boldsymbol{\Gamma}.
\end{aligned} \tag{39}$$

It is observed that, while the matrix $\boldsymbol{D}_2\left(\mathring{N}\right)$ is symmetric, the matrices $\boldsymbol{D}_1\left(\mathring{N}, \mathring{N}'\right)$ and $\boldsymbol{D}_0\left(\mathring{N}, \mathring{N}'\right)$ calls for the following discussion: (a) in the case in which $\mathring{N}' = 0$ (i.e., the self-weight is absent), $\boldsymbol{D}_1\left(\mathring{N}, 0\right)$ is skew-symmetric and $\boldsymbol{D}_0\left(\mathring{N}, 0\right)$ is symmetric; (b) if $\mathring{N}' \neq 0$ (self-weigh does exist), then $\boldsymbol{D}_1\left(\mathring{N}, \mathring{N}'\right)$ and $\boldsymbol{D}_0\left(\mathring{N}, \mathring{N}'\right)$ are neither symmetric nor skew-symmetric. In spite of this occurrence, it is easy to check that the differential equations (35) (as well the boundary conditions (36)) are *self-adjoint*, since the following Green Identity holds:

$$\int_0^\ell \boldsymbol{v}^T\left(\boldsymbol{D}_2\boldsymbol{u}'' + \boldsymbol{D}_1\boldsymbol{u}' + \boldsymbol{D}_0\boldsymbol{u}\right)\mathrm{d}s = \int_0^\ell \boldsymbol{u}^T\left(\boldsymbol{D}_2\boldsymbol{v}'' + \boldsymbol{D}_1\boldsymbol{v}' + \boldsymbol{D}_0\boldsymbol{v}\right)\mathrm{d}s + \text{boundary conditions}, \tag{40}$$

consistently with the conservative nature of forces and constitutive law.

Bifurcation parameters

The boundary value problem (35), (36) depends on two bifurcation parameters, the tip force F and the floor self-weight W. It is convenient to introduce two nondimensional load parameters μ, ν such that $F = \mu P_c^\star$, $W = \nu P_c^\star / \left(\frac{1}{2} + \frac{\ell}{h}\right)$, with $P_c^\star$ the critical load of a single cell. Accordingly, from Eq (6):

$$\mathring{N}(s) := -\left(\mu + \nu\, f\,(s)\right) P_c^\star, \qquad f\,(s) := 1 - \frac{2\,s}{h + 2\,\ell}, \tag{41}$$

so that the boundary value problem reads:

$$\begin{aligned}
&\left(\boldsymbol{D}_2^0 - \left(\mu + \nu\, f\,(s)\right)\hat{\boldsymbol{D}}_2^\star\right)\boldsymbol{u}'' + \left(\boldsymbol{D}_1^0 - \left(\mu + \nu\, f\,(s)\right)\hat{\boldsymbol{D}}_1^\star - \nu f'\,(s)\,\check{\boldsymbol{D}}_1^\star\right)\boldsymbol{u}' \\
&\quad + \left(\boldsymbol{D}_0^0 - \left(\mu + \nu\, f\,(s)\right)\hat{\boldsymbol{D}}_0^\star - \nu f'\,(s)\,\check{\boldsymbol{D}}_0^\star\right)\boldsymbol{u} = \boldsymbol{0}, \\
&\boldsymbol{A}_u\boldsymbol{u}_A = \boldsymbol{0}, \\
&\left(\boldsymbol{B}_{H1}^0 - \left(\mu + \nu\, f\,(s_H)\right)\hat{\boldsymbol{B}}_{H1}^\star\right)\boldsymbol{u}_H' + \left(\boldsymbol{B}_{H0}^0 - \left(\mu + \nu\, f\,(s_H)\right)\hat{\boldsymbol{B}}_{H0}^\star\right)\boldsymbol{u}_H = \boldsymbol{0}, \qquad H = A, B,
\end{aligned} \tag{42}$$

where the following positions hold:

$$\begin{aligned}
\hat{\boldsymbol{D}}_i^\star &:= P_c^\star\hat{\boldsymbol{D}}_i, \qquad i = 0, 1, 2, \\
\check{\boldsymbol{D}}_i^\star &:= P_c^\star\check{\boldsymbol{D}}_i, \qquad i = 0, 1, \\
\hat{\boldsymbol{B}}_{Hj}^\star &:= P_c^\star\hat{\boldsymbol{B}}_{Hj}, \quad j = 0, 1.
\end{aligned} \tag{43}$$

The combinations $(\mu, \nu) = (\mu_c, \nu_c)$ for which the boundary value problem (42) admits nontrivial solutions, identify states of incipient instability for the beam. For any given ratio $\rho := \mu/\nu$, the pair (μ_c, ν_c) of smallest modulus $\min_{\rho=\text{const}} \left(\sqrt{\mu^2+\nu^2}\right) = \sqrt{\mu_c^2+\nu_c^2}$ will be denoted as the *critical* load combination. As an algorithmic strategy, a set of values of ρ is chosen, and, for each of them, the bifurcation parameters are proportionally increased from zero, until the condition of static bifurcation (a zero eigenvalue) is encountered first. The collection of the critical states (μ_c, ν_c) for different ρ values is a geometrical locus on the (μ, ν)-plane, which is the boundary of the stability domain of the beam.

Finite difference solution

Since the boundary value problem (42) has variable coefficients, it cannot be solved in closed form. An exception occurs when self-weight is not present, for which a closed form exists, determined in [24] for the case of rigid soil, and easily adaptable to the case of elastic soil, at hand. Here, addressing the more general case of self-weight, the problem is attacked by the finite difference method.

Accordingly, the domain $[0, \ell]$ is divided in L elements and $L+1$ nodes of coordinates $s_i = i\Delta$ $(i = 0, 1, \ldots, L)$, with $\Delta := \ell/L$. Two dummy nodes -1, $L+1$ are added, of coordinates $s_{-1} = -\Delta$ and $s_{L+1} = (L+1)\,\Delta$. By using central finite differences, the derivatives are approximated as follows:

$$\begin{aligned} \boldsymbol{u}_i &= \boldsymbol{u}\,(s_i)\,, \\ \boldsymbol{u}_i' &= \frac{\boldsymbol{u}_{i+1} - \boldsymbol{u}_{i-1}}{2\Delta}, \\ \boldsymbol{u}_i'' &= \frac{\boldsymbol{u}_{i+1} - 2\boldsymbol{u}_i + \boldsymbol{u}_{i-1}}{\Delta^2}. \end{aligned} \tag{44}$$

Hence, the boundary value problem (42) is transformed as follows into an algebraic problem[1]:

$$\begin{aligned} &\boldsymbol{A}_u \boldsymbol{u}_0 = \boldsymbol{0}, \\ &\left(\boldsymbol{B}_{A1}^0 - (\mu + \nu\, f_0)\, \hat{\boldsymbol{B}}_{A1}^\star\right) \frac{\boldsymbol{u}_1 - \boldsymbol{u}_{-1}}{2\Delta} + \left(\boldsymbol{B}_{A0}^0 - (\mu + \nu\, f_0)\, \hat{\boldsymbol{B}}_{A0}^\star\right) \boldsymbol{u}_0 = \boldsymbol{0}, \\ &\left(\boldsymbol{D}_2^0 - (\mu + \nu\, f_i)\, \hat{\boldsymbol{D}}_2^\star\right) \frac{\boldsymbol{u}_{i+1} - 2\boldsymbol{u}_i + \boldsymbol{u}_{i-1}}{\Delta^2} + \left(\boldsymbol{D}_1^0 - (\mu + \nu\, f_i)\, \hat{\boldsymbol{D}}_1^\star - \nu f_i'\, \check{\boldsymbol{D}}_1^\star\right) \frac{\boldsymbol{u}_{i+1} - \boldsymbol{u}_{i-1}}{2\Delta} \\ &+ \left(\boldsymbol{D}_0^0 - (\mu + \nu\, f_i)\, \hat{\boldsymbol{D}}_0^\star - \nu f_i'\, \check{\boldsymbol{D}}_0^\star\right) \boldsymbol{u}_i = \boldsymbol{0}, \qquad i = 0, \ldots, L, \\ &\left(\boldsymbol{B}_{B1}^0 - (\mu + \nu\, f_L)\, \hat{\boldsymbol{B}}_{B1}^\star\right) \frac{\boldsymbol{u}_{L+1} - \boldsymbol{u}_{L-1}}{2\Delta} + \left(\boldsymbol{B}_{B0}^0 - (\mu + \nu\, f_L)\, \hat{\boldsymbol{B}}_{B0}^\star\right) \boldsymbol{u}_L = \boldsymbol{0}, \end{aligned} \tag{46}$$

where $f_i := f\,(s_i)$, $f_i' := f'\,(s_i)$. Equations can be recast in the form:

$$\left(\mathsf{K}_0 - \mu \mathsf{K}_\mu - \nu \mathsf{K}_\nu\right) \mathsf{u} = \boldsymbol{0}, \tag{47}$$

where $\mathsf{u} = (\boldsymbol{u}_{-1}, \boldsymbol{u}_0, \cdots, \boldsymbol{u}_L, \boldsymbol{u}_{L+1})^T$, K_0 is the elastic matrix and K_μ, K_ν are geometric stiffness matrices, all of dimension $6\,(L+3) \times 6\,(L+3)$. By letting $\nu = \rho\mu$ for chosen ρ's, Eq (47) is an eigenvalue problem, in non-standard form, for the eigenvalue μ. The smallest positive value μ_c is the critical load, associated with $\nu_c = \rho\mu_c$.

4 Numerical results

Numerical results, concerning buckling of different buildings taken as case studies, are presented and discussed. Aimed at investigating the effectiveness of the equivalent Timoshenko beam, results are compared with those obtained by benchmark finite-element analyses (FEA), in which the buildings are modeled as 3D-frames.

[1] It should be remarked that, when the rigid soil is considered, i.e., the beam is clamped at A, the first two equations (46) must be replaced by:

$$\boldsymbol{u}_0 = \boldsymbol{0} \tag{45}$$

the dummy node -1 suppressed, and the third of (46) has to be evaluated in the interval $i = 1, \ldots, L$.

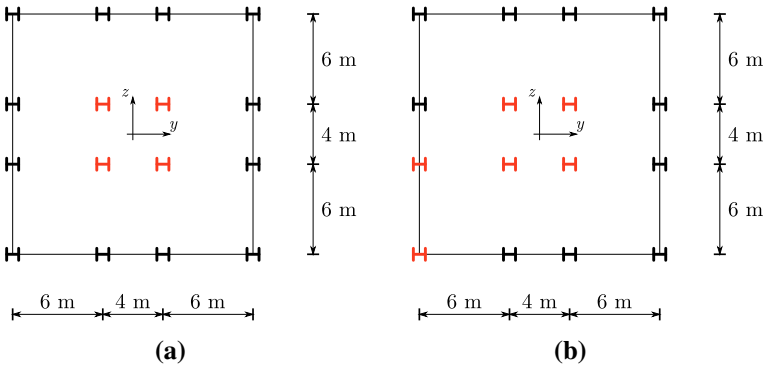

Fig. 2 Case studies: **a** bi-symmetric column layout; **b** asymmetric column layout

Table 1 Cross sections properties

	A $[\mathrm{m}^2]$	I_y $[\mathrm{m}^4]$	I_z $[\mathrm{m}^4]$	J $[\mathrm{m}^4]$	A_y $[\mathrm{m}^2]$	A_z $[\mathrm{m}^2]$
Type i	1.06×10^{-2}	6.301×10^{-5}	1.728×10^{-4}	5.852×10^{-7}	2.456×10^{-3}	7×10^{-3}
Type ii	1.53×10^{-2}	8.554×10^{-5}	4.326×10^{-4}	1.47×10^{-6}	4.29×10^{-3}	9.5×10^{-3}

Buildings with the columns' layouts displayed in Fig. 2 are considered, having the same arrangement, but with the individual columns having different geometric characteristics. The case studies are:

– case study I (Fig. 2a), concerning a bi-symmetric layout;
– case study II (Fig. 2b), concerning an asymmetric layout;

the columns' I-shape cross sections are defined as: type *i* (black in Fig. 2) or type *ii* (red in Fig. 2), whose geometrical properties are reported in Table 1. The inter-floor height is taken as $h = 4\,\mathrm{m}$, but the number of floors n is considered as a variable parameter.

The considered material for both types of column is steel, having Young modulus $E = 2 \times 10^8\ \mathrm{kN/m^2}$ and shear modulus $G = 7.69 \times 10^7\ \mathrm{kN/m^2}$. The elasto-geometric characteristics of the Timoshenko beam are reported in Table 2 for each case study. Finally, the Winkler's soil elastic constant is taken as $k_s = 30 \times 10^3\ \mathrm{kN/m^3}$, which corresponds to a compact clay. By considering a square foundation of side 16 m, whose principal inertia axes are aligned with those of the generic floor, it follows that (see Appendix B) $k_x = 7.68 \times 10^6\ \mathrm{kN/m}$, $k_y = k_z = 163.84 \times 10^6\ \mathrm{kNm}$, $k_{yz} = 0$. In the following numerical simulations, the equivalent model domain has been discretized with 200 elements, according to the finite-difference scheme, described in Sect. 3.

Buckling of buildings under tip load

Buckling induced by a tip load, in the symmetric case study I, is first addressed. The influence of the number of floors, with or without soil elasticity, is investigated. The equivalent model has been used for this purposes, by solving the finite-difference discretized problem (47). Results of this analysis are displayed in Fig. 3. It is seen that the critical buckling load multiplier μ decreases with the number of floors n, in a pattern similar to the well-known one of the Timoshenko beam. The elastic soil (light blue curve in the figure), slightly modifies the behavior of a clamped (rigid soil) building, as predicted by the order-of-magnitude analysis developed in Sect. 2.

In the same Fig. 3, three different number of floors (green dots labeled with numbers 1, 2, 3, corresponding to $n = 10,\ 50,\ 100$, respectively) are selected, to compare the equivalent model solution with that furnished by finite-element discretization on a fine model. Comparison is shown in Fig. 4 in terms of displacement components of the critical mode of the three buildings of different height. It is seen that the continuous curves, representing the Timoshenko equivalent model in the clamped (black lines) and elastic soil (light blue lines) cases, are almost superimposed on the dots and circles, which instead represent the correspondent FE solutions. In all the cases, the critical mode is an 'Euler-type' flexural mode, occurring in the weaker plane of inertia, and its shape is found to be independent on the number of floors. Only when the number of floors is sufficiently

Table 2 Elasto-geometric coefficients of the Timoshenko beam model for the case study I and II

		Case I	Case II
D	[kN/m]	9.42×10^6	9.89×10^6
S_y	[kN/m]	1.226×10^5	1.383×10^5
S_z	[kN/m]	4.048×10^4	4.214×10^4
C	[kN × m]	4.502×10^6	5.143×10^6
B_y	[kN × m]	2.921×10^8	3.081×10^8
B_z	[kN × m]	2.922×10^8	3.224×10^8
B_{yz}	[kN × m]	0	1.88×10^7
y_S	[m]	0	−0.315
z_S	[m]	0	−0.568
y_E	[m]	0	−0.380
z_E	[m]	0	−0.238
$\hat{C}_{22}$	[−]	1.131	1.128
$\hat{C}_{24}$	[m]	0	−0.018
$\hat{C}_{26}$	[m]	2	2
$\hat{C}_{33}$	[−]	1.193	1.193
$\hat{C}_{34}$	[m]	0	0
$\hat{C}_{35}$	[m]	−2	−2
$\hat{C}_{44}$	$[m^2]$	72.301	73.934
$\hat{C}_{55}$	$[m^2]$	5.333	5.333
$\hat{C}_{66}$	$[m^2]$	5.333	5.333

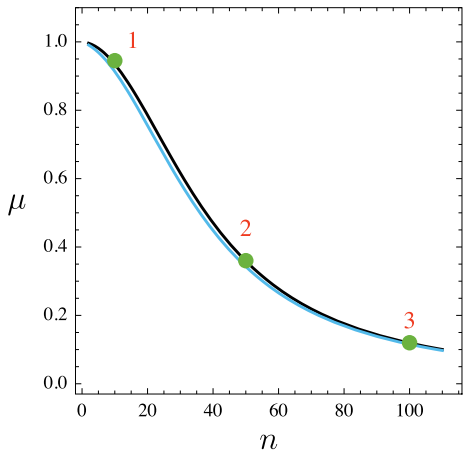

Fig. 3 Critical load multiplier μ vs number of floors, for the case study I. Clamped case in continuous black line, elastically restrained case in light blue line. Green dots: selected number of floors for comparison with FE solution (colour figure online)

small, i.e., $n = 10$, some appreciable difference between clamped and elastic soil cases is detected, as it is predicted by the order-of-magnitude analysis. Finally, the percentage error on the critical load multiplier of the equivalent model, when compared with that of FE solution, is about 1% (results not reported here).

Buckling of buildings under uniformly distributed load

The buckling of the same building defined in case study I, but under only distributed loads, is studied here. Results of the analysis are displayed in Fig. 5 in terms of the nondimensional normal force at ground, $\nu = -\mathring{N}(0)/P_c^\star$ (remember Eq. (41)), for different number of floors. It is seen that, below a threshold number of floors, the critical normal force remains constant, equal to the critical load of the cell. However, when this floor number is exceeded, the critical force at the ground decreases with increasing n. This circumstance is explained by the nature of the critical mode, which is (i) localized at the bottom of the building, when n is

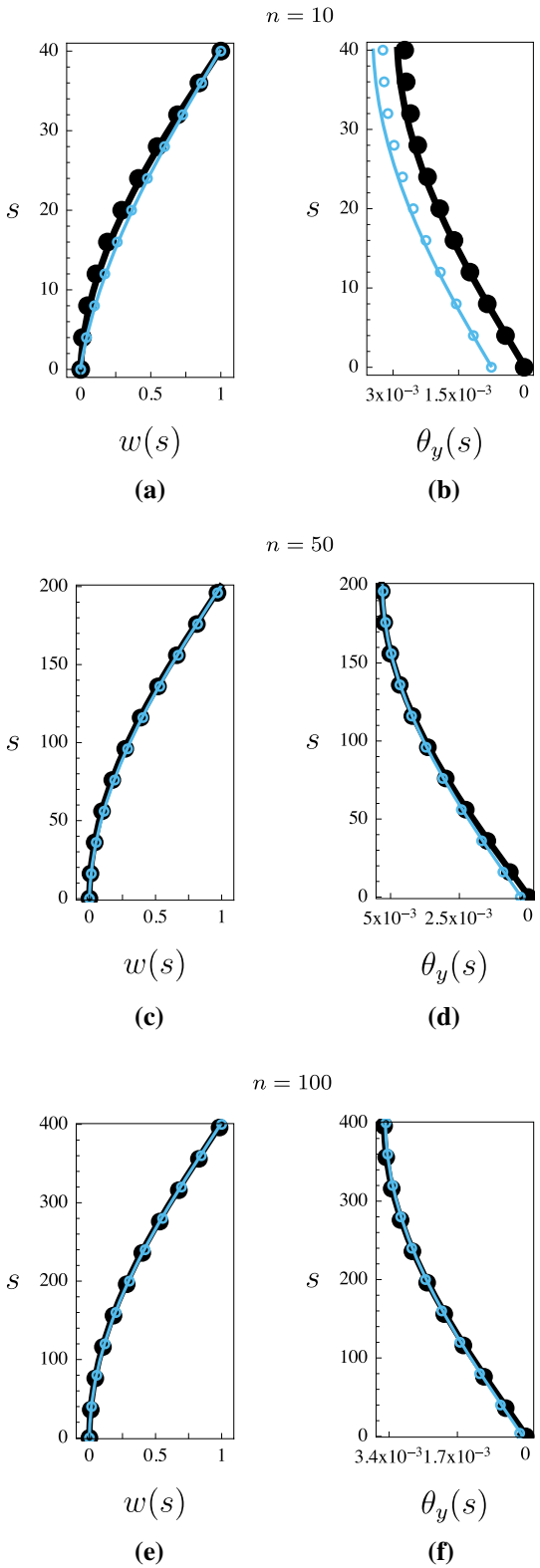

Fig. 4 Critical mode in the case study I, under tip force, for different number of floors, namely: **a**, **b** $n = 10$; **c**, **d** $n = 50$; (e), (f) $n = 100$. Rigid soil in black; elastic soil in light blue. Continuous lines: Timoshenko model; dots and circles: FE solution (colour figure online)

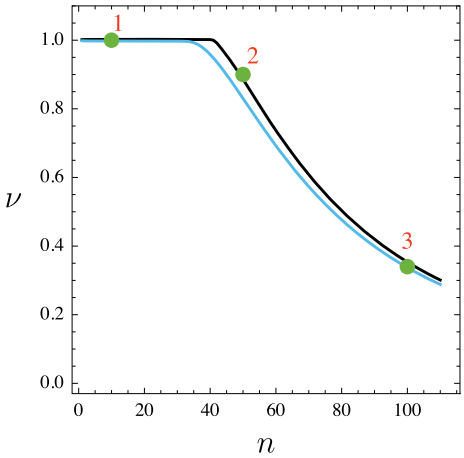

Fig. 5 Nondimensional ground normal force ν versus number of floors, for the case study I. Clamped case in continuous black line, elastically restrained case in light blue line. Green dots: selected number of floors for comparison with FE solution (colour figure online)

small, and (ii) is of global type, when n is large. Also in this case, the effect of the elastic soil (light blue curve in the figure) slightly changes the behavior of clamped buildings (rigid soil).

The local or global character of the critical mode is illustrated in Fig. 6, for buildings of different height (marked with green dots and numbers 1, 2 and 3 in Fig. 5, having $n = 10,\ 50,\ 100$ floors, respectively). The critical mode is: (i) localized when $n = 10$; (ii) global, of 'Timoshenko-type,' when $n = 50$; and, (iii) of global, of 'Euler-type,' when $n = 100$. In general, an excellent agreement between the equivalent beam and the FEM model is found, in except for the case of localized mode and elastic soil, where a significant difference is found. However, the description of localized modes is out of the goal of this paper, since the equivalent model is developed to describe global and not local phenomena. Finally, the percentage error on the critical load multiplier of the equivalent model, compared to that of the FE solution, is less than 3% (results not reported here).

Buckling of buildings under combined tip and uniformly distributed loads

The combined effect of the two loads, lumped and distributed, is now investigated, for the two case studies, I and II, and different number of floors ($n = 10, 50, 100$, labeled as 1, 2, 3, respectively).

Results for case-I are shown in Fig. 7, where the interaction domain, μ vs ν, is displayed for the three different buildings. In this figure, the black lines are referred to clamped equivalent Timoshenko beam, while the light-blue lines are relevant to the same beam, but elastically restrained. Each curve represents the boundary of stability domain, i.e., the locus of the critical parameters (μ, ν) which entails incipient instability of the building. States of load represented by points of the plane which are on the left of each locus (denoted with S for the case 1 in the figure), are stable; the other states are unstable (denoted with U for the case 1 in the figure).

In Fig. 8, the analysis for the case study II, with $n = 20$, rigid soil, and with a state of load characterized by the ratio $\nu/\mu = 0.287$, is illustrated. The results of this model are in excellent agreement with those of the FEM analyses, both in terms of critical mode and (see Fig. 8) in terms of magnitude of critical load multiplier. It is important to remark that in this case, due to the asymmetry in the column layout, all displacement components of the critical mode are nonzero, entailing a flexural–torsional behavior of the building.

5 Conclusions

The buckling behavior of tower buildings, uniformly and not uniformly compressed, has been addressed in this paper. To this end an equivalent Timoshenko beam model, embedded in a three-dimensional space, and accounting for the geometric effect of compression, has been formulated in the framework of up-scaling methods. Homogenization has been carried out coupling heuristic approaches and asymptotic homogenization

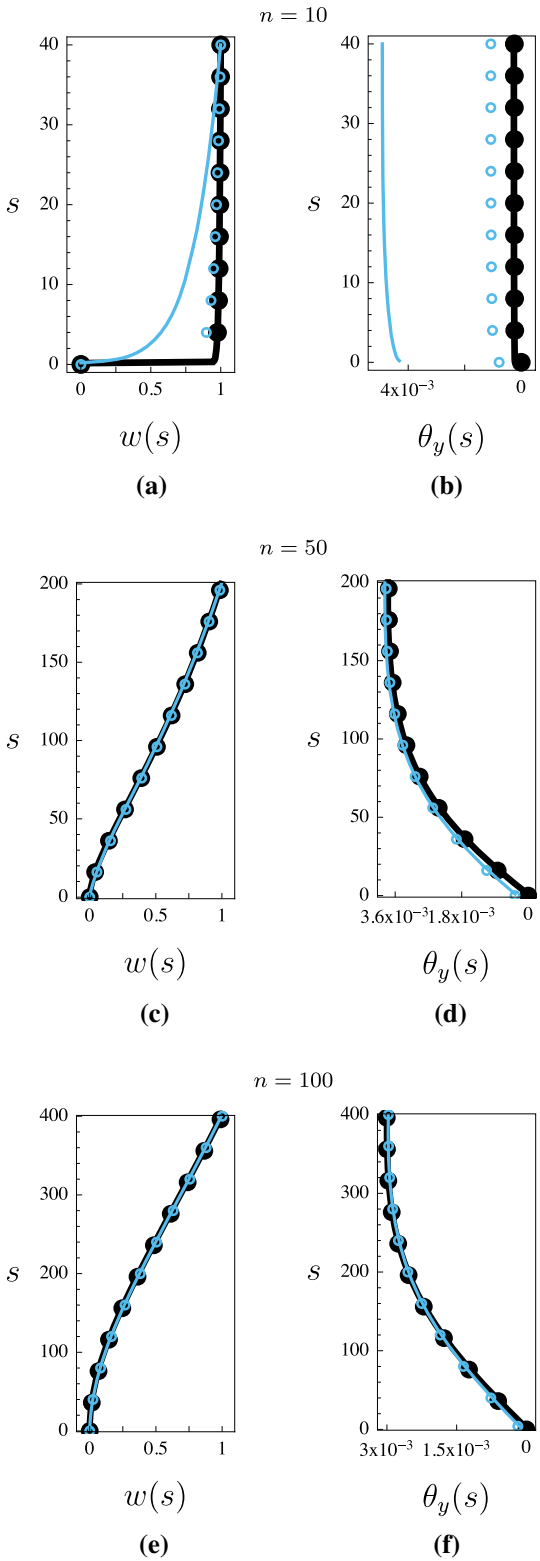

Fig. 6 Critical mode in the case study I, under uniformly distributed load, for different number of floors, namely: **a**, **b** $n = 10$; **c**, **d** $n = 50$; **e**, **f** $n = 100$. Rigid soil in black; elastic soil in light blue. Continuous lines: Timoshenko model; dots and circles: FE solution

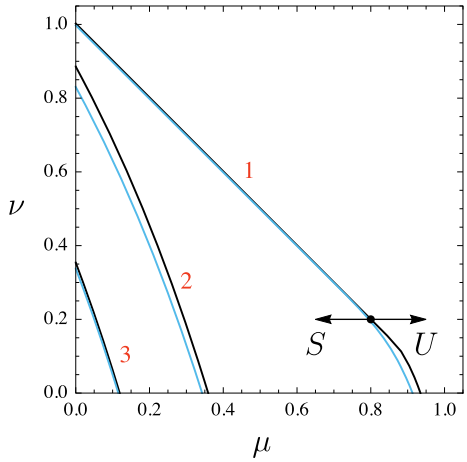

Fig. 7 Interaction domains of the two bifurcation parameters for the case study I and for $n = 10$ (curves 1), $n = 50$ (curves 2), $n = 100$ (curves 3). Clamped case in continuous black line, elastically restrained case in light blue line

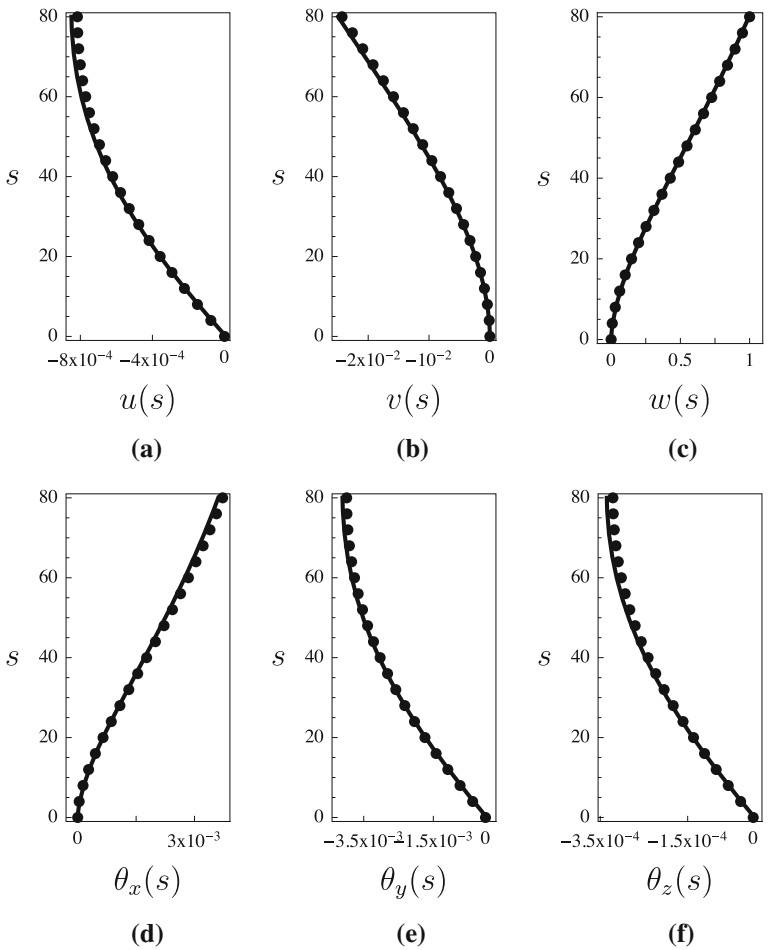

Fig. 8 Critical mode in the case study II, under combined tip and distributed loads. For Timoshenko model: clamped case in continuous black line. For FE solution: black dots

methods. All the results, given by the equivalent continuous model, have been compared with those obtained through finite-element analyses carried out on three-dimensional frames. The bifurcation analysis of the equivalent model, governed by a boundary value problem with variable coefficients, has been performed through

a numerical discretization, grounded on the finite difference method, also accounting for the interaction with a Winkler-type soil, and for both symmetric and asymmetric layout of the columns of the tower building. An order-of-magnitude analysis has been carried out to predict the influence of the soil in changing the elastic behavior of the building. The following conclusions can be drawn.

1. The geometric effect of the prestress affects both equilibrium and constitutive equations of the 1D equivalent model. The second aspect models microscopic effects which could not be accounted for on the macroscopic scale.
2. In the case of tip load, the shape of buckling mode is of 'Euler-type,' and it does not change with the number of floors.
3. In the case of uniformly distributed load, the buckling mode, has a 'Local-' or a 'Timoshenko-' and 'Euler-type' buckling shape, as the floor number increases.
4. In general, soil does not change, both qualitatively nor qualitatively, the buckling behavior of tower buildings, as predicted by the order-of-magnitude analysis. In particular, some significant quantitative effects can be recognized in the buckling mode only when the number of floors is sufficiently small.
5. Flexural–torsional buckling modes have been detected when the columns layout is not symmetric.
6. The model permits to account for combined actions of tip and uniformly distributed loads; it supplies interaction domains, useful for design purposes.
7. A very good agreement between the critical loads and modes of the equivalent beam, with respect to benchmark solutions, obtained via finite-element analyses has been found, when the buckling mode has global character.
8. Remarkably, a lower computational effort in managing the equivalent one-dimensional beam model has been experienced, with respect to refined frame models of buildings in a three-dimensional space.

Acknowledgements Open access funding provided by Università degli Studi dell'Aquila within the CRUI-CARE Agreement.

A Stiffnesses of the springs representative of the soil

In order to evaluated the elastic stiffness representative of the behavior of the foundation, it is assumed that the centroid of the ground floor, is coincident with that of the foundation, i.e., $A \equiv G$. Moreover, the foundation is modeled as a rigid body, for which the transverse displacement of a generic point P on it, reads:

$$u = u_A - \theta_{zA} y + \theta_{yA} z, \tag{48}$$

u_A, θ_{zA}, θ_{yA}, being the displacements of the centroid of the ground floor. The elastic (and uniformly distributed on the foundation) reaction of the linear soil is assumed to be directed towards axis $\bar{\mathbf{a}}_x$, whose magnitude σ_x is:

$$\sigma_x = -k_s\, u, \tag{49}$$

k_s being the Winkler's soil elastic constant.

The resultant actions (forces and moments) on the foundation, therefore, read:

$$\begin{aligned} F_x^{el} &= \int_{\mathcal{A}} \sigma_x \, dA = -k_x u_A, \\ C_y^{el} &= \int_{\mathcal{A}} \sigma_x z \, dA = -k_y \theta_{yA} + k_{yz} \theta_{zA}, \\ C_z^{el} &= -\int_{\mathcal{A}} \sigma_x y \, dA = k_{yz} \theta_{yA} - k_z \theta_{zA}, \end{aligned} \tag{50}$$

where, F_x^{el} is the magnitude of the elastic vertical force and C_y^{el}, C_z^{el} are the magnitudes of the elastic moments of axes y and z, respectively[2]. Moreover, the following definitions of the elastic coefficients of the springs, are introduced:

$$\begin{aligned} k_x &= k_s\, A_f, \\ k_y &= k_s \int_{\mathcal{A}_f} z^2\, dA = k_s\, I_y, \\ k_z &= k_s \int_{\mathcal{A}_f} y^2\, dA = k_s\, I_z, \\ k_{yz} &= k_s \int_{\mathcal{A}_f} yz\, dA = k_s\, I_{yz}, \end{aligned} \tag{51}$$

A_f, I_y, I_z, and I_{yz} being the area and the moments of inertia of the foundation, respectively.

B Expressions of the elastic matrices

Elastic matrices, appearing in Eqs. (28) and (29), read:

$$\mathbf{K}_i^0 = \begin{pmatrix} D_i & 0 & 0 & 0 & 0 & 0 \\ & S_{iy} & 0 & 0 & 0 & -\frac{hS_{iy}}{2} \\ & & S_{iz} & 0 & \frac{hS_{iz}}{2} & 0 \\ & & & C_i & 0 & 0 \\ & & & & \frac{\alpha_{iy}+4}{\alpha_{iy}+1} B_{iy} & 0 \\ \text{SYM} & & & & & \frac{\alpha_{iz}+4}{\alpha_{iz}+1} B_{iz} \end{pmatrix},$$

$$\hat{\mathbf{K}}_i = \begin{pmatrix} 0 & 0 & 0 & 0 & 0 & 0 \\ & \frac{2(5\alpha_{iz}+3)}{5h(\alpha_{iz}+1)^2} & 0 & 0 & 0 & \frac{5\alpha_{iz}^2-1}{10(\alpha_{iz}+1)^2} \\ & & \frac{2(5\alpha_{iy}+3)}{5h(\alpha_{iy}+1)^2} & 0 & \frac{1-5\alpha_{iy}^2}{10(\alpha_{iy}+1)^2} & 0 \\ & & & 0 & 0 & 0 \\ & & & & h\frac{4-5(\alpha_{iy}-1)\alpha_{iy}}{30(\alpha_{iy}+1)^2} & 0 \\ \text{SYM} & & & & & h\frac{4-5(\alpha_{iz}-1)\alpha_{iz}}{30(\alpha_{iz}+1)^2} \end{pmatrix}, \tag{52}$$

$$\mathbf{C}^0 := h \begin{pmatrix} D & 0 & 0 & 0 & D\, z_E & -D\, y_E \\ & S_y & 0 & -S_y\, z_S & 0 & 0 \\ & & S_z & S_z\, y_S & 0 & 0 \\ & & & C & 0 & 0 \\ & & & & B_y & -B_{yz} \\ \text{SYM} & & & & & B_z \end{pmatrix},$$

$$\hat{\mathbf{C}} := \begin{pmatrix} 0 & 0 & 0 & 0 & 0 & 0 \\ & \hat{C}_{22} & 0 & \hat{C}_{24} & 0 & \hat{C}_{26} \\ & & \hat{C}_{33} & \hat{C}_{34} & \hat{C}_{35} & 0 \\ & & & \hat{C}_{44} & 0 & 0 \\ & & & & \hat{C}_{55} & 0 \\ \text{SYM} & & & & & \hat{C}_{66} \end{pmatrix},$$

[2] It is important to remark that, if the axes y and z are principal of inertia for the foundation, the flexural coupling governed by k_{yz} is zero.

where the following elastic coefficients for the generic i-th column are introduced:

$$\begin{aligned} D_i &= \frac{EA_i}{h}, \quad S_{iy} = \frac{12EI_{iz}}{(1+\alpha_{iz})\,h^3}, \quad B_{iy} = \frac{EI_{iy}}{h}, \\ C_i &= \frac{GJ_i}{h}, \quad S_{iz} = \frac{12EI_{iy}}{\left(1+\alpha_{iy}\right)h^3}, \quad B_{iz} = \frac{EI_{iz}}{h}, \end{aligned} \tag{53}$$

in which the flexural-to-shear stiffness ratios appear:

$$\alpha_{iz} := \frac{12EI_{iz}}{GA_{iy}h^2}, \quad \alpha_{iy} := \frac{12EI_{iy}}{GA_{iz}h^2}. \tag{54}$$

Moreover, the elastic coefficients for the coarse model reads:

$$\begin{aligned} &D := \sum_{i=1}^{N} D_i, && y_E := \frac{1}{D}\sum_{i=1}^{N} D_i y_i, && z_E := \frac{1}{D}\sum_{i=1}^{N} D_i z_i, && S_y := \sum_{i=1}^{N} S_{iy}, \\ &S_z := \sum_{i=1}^{N} S_{iz}, && y_S := \frac{1}{S_z}\sum_{i=1}^{N} S_{iz} y_i, && z_S := \frac{1}{S_y}\sum_{i=1}^{N} S_{iy} z_i, && C := \sum_{i=1}^{N} C_i + S_{iz}y_i^2 + S_{iy}z_i^2, \\ &B_y := \sum_{i=1}^{N} B_{iy} + D_i z_i^2, && B_z := \sum_{i=1}^{N} B_{iz} + D_i y_i^2, && B_{yz} := \sum_{i=1}^{N} D_i y_i z_i, && \beta_{iy} := \frac{6+10\,\alpha_{iz}}{5\,(1+\alpha_{iz})^{\,2}}, \\ &\beta_{iz} := \frac{6+10\,\alpha_{iy}}{5\left(1+\alpha_{iy}\right)^{2}}, && \hat{C}_{22} := \sum_{i=1}^{N} \beta_{iy}\eta_i, && \hat{C}_{24} := -\sum_{i=1}^{N} \beta_{iy}\eta_i z_i, && \hat{C}_{26} := h/2, \\ &\hat{C}_{33} = \sum_{i=1}^{N} \beta_{iz}\eta_i, && \hat{C}_{34} := \sum_{i=1}^{N} \beta_{iz}\eta_i y_i, && \hat{C}_{35} := -\hat{C}_{26}, && \hat{C}_{44} := \sum_{i=1}^{N} \eta_i \left(\beta_{iz}y_i^2 + \beta_{iy}z_i^2\right), \\ &\hat{C}_{55} := h^2/3, && \hat{C}_{66} := \hat{C}_{55}, && \eta_i := D_i\left(\hat{u}_G - \hat{\theta}_z y_i + \hat{\theta}_y z_i\right). \end{aligned} \tag{55}$$

where the following coefficients, representing the displacements of the centroid of the cell's rigid floor, when a normal unitary vertical load is applied on it, are defined:

$$\begin{aligned} \hat{u}_G &:= \frac{B_{yz}^2 - \hat{B}_y\hat{B}_z}{D\left[B_{yz}^2 - \hat{B}_y\hat{B}_z + D\left(\hat{B}_y y_E^2 - 2B_{yz}y_E z_E + \hat{B}_z z_E^2\right)\right]}, \\ \hat{\theta}_y &:= \frac{\hat{B}_z z_E - B_{yz}y_E}{B_{yz}^2 - \hat{B}_y\hat{B}_z + D\left(\hat{B}_y y_E^2 - 2B_{yz}y_E z_E + \hat{B}_z z_E^2\right)}, \\ \hat{\theta}_z &:= \frac{B_{yz}z_E - \hat{B}_y y_E}{B_{yz}^2 - \hat{B}_y\hat{B}_z + D\left(\hat{B}_y y_E^2 - 2B_{yz}y_E z_E + \hat{B}_z z_E^2\right)}. \end{aligned} \tag{56}$$

Moreover:

$$\hat{B}_y := \sum_{i=1}^{N} D_i z_i^2, \quad \hat{B}_z := \sum_{i=1}^{N} D_i y_i^2, \tag{57}$$

are the bending stiffnesses of the beam-like structure, with the column flexural stiffnesses ignored.

References

1. Bui, Q.-B., Hans, S., Boutin, C.: Dynamic behaviour of an asymmetric building: experimental and numerical studies. Case Stud. Nondestruct. Test. Eval. **2**, 38–48 (2014)
2. Kim, H.-S., Lee, D.-G., Kim, C.K.: Efficient three-dimensional seismic analysis of a high-rise building structure with shear walls. Eng. Struct. **27**(6), 963–976 (2005)

3. Liu, H., Yang, Z., Gaulke, M.S.: Structural identification and finite element modeling of a 14-story office building using recorded data. Eng. Struct. **27**(3), 463–473 (2005)
4. Boutin, C., Hans, S., Chesnais, C.: Generalized Beams and Continua. Dynamics of Reticulated Structures, pp. 131–141. Springer New York, New York, NY (2010)
5. Luongo, A., Zulli, D.: Mathematical Models of Beams and Cables. Wiley, Hoboken (2013)
6. Giorgio, I., Rizzi, N.L., Turco, E.: Continuum modelling of pantographic sheets for out-of-plane bifurcation and vibrational analysis. Proc. R. Soc. A: Math. Phys. Eng. Sci. **473**(2207), 20170636 (2017)
7. Andreaus, U., Spagnuolo, M., Lekszycki, T., Eugster, S.R.: A Ritz approach for the static analysis of planar pantographic structures modeled with nonlinear Euler–Bernoulli beams. Continuum Mech. Thermodyn. **30**(5), 1103–1123 (2018)
8. dell'Isola, F., Seppecher, P., Spagnuolo, M., et al.: Advances in pantographic structures: design, manufacturing, models, experiments and image analyses. Continuum Mech. Thermodyn. **31**(4), 1231–1282 (2019a)
9. dell'Isola, F., Seppecher, P., Alibert, J.J., et al.: Pantographic metamaterials: an example of mathematically driven design and of its technological challenges. Continuum Mech. Thermodyn. **31**(4), 851–884 (2019b)
10. De Angelo, M., Barchiesi, E., Giorgio, I., Abali, B.E.: Numerical identification of constitutive parameters in reduced-order bi-dimensional models for pantographic structures: application to out-of-plane buckling. Arch. Appl. Mech. **89**(7), 1333–1358 (2019)
11. Boutin, C., Hans, S.: Homogenisation of periodic discrete medium: application to dynamics of framed structures. Comput. Geotech. **30**(4), 303–320 (2003)
12. Hans, S., Boutin, C.: Dynamics of discrete framed structures: a unified homogenized description. J. Mech. Mater. Struct. **3**(9), 1709–1739 (2008)
13. Chesnais, C., Boutin, C., Hans, S.: Structural Dynamics and Generalized Continua, pp. 57–76. Springer, Berlin (2011)
14. Cluni, F., Gioffrè, M., Gusella, V.: Dynamic response of tall buildings to wind loads by reduced order equivalent shear-beam models. J. Wind Eng. Ind. Aerodyn. **123**, 339–348 (2013)
15. Piccardo, G., Tubino, F., Luongo, A.: A shear-shear torsional beam model for nonlinear aeroelastic analysis of tower buildings. Z. Angew. Math. Phys. **66**(4), 1895–1913 (2015)
16. Piccardo, G., Tubino, F., Luongo, A.: Equivalent nonlinear beam model for the 3-d analysis of shear-type buildings: application to aeroelastic instability. Int. J. Non-Linear Mech. **80**, 52–65 (2016)
17. Piccardo, G., Tubino, F., Luongo, A.: Equivalent timoshenko linear beam model for the static and dynamic analysis of tower buildings. Appl. Math. Model. **71**, 77–95 (2019)
18. Potzta, G., Kollár, L.P.: Analysis of building structures by replacement sandwich beams. Int. J. Solids Struct. **40**(3), 535–553 (2003)
19. Zalka, K.A.: Global Structural Analysis of Buildings. CRC Press, Boca Raton (2002a)
20. Di Nino, S., Luongo, A.: Nonlinear aeroelastic behavior of a base-isolated beam under steady wind flow. Int. J. Non-Linear Mech. **119**, 103340 (2020)
21. Luongo, A., Zulli, D.: Free and forced linear dynamics of a homogeneous model for beam-like structures. Meccanica **55**, 1–19 (2019)
22. Zalka, K.A.: Mode coupling in the torsional-flexural buckling of regular multistorey buildings. Struct. Des. Tall Spec. Build. **3**(4), 227–245 (1994)
23. Zalka, K.A.: Buckling analysis of buildings braced by frameworks, shear walls and cores. Struct. Des. Tall Spec. Build. **11**(3), 197–219 (2002b)
24. Ferretti, M.: Flexural torsional buckling of uniformly compressed beam-like structures. Continuum Mech. Thermodyn. **30**(5), 977–993 (2018)
25. Noor, A.K.: Continuum modeling for repetitive lattice structures. Appl. Mech. Rev. **41**(7), 285–296 (1988)
26. Tollenaere, H., Caillerie, D.: Continuous modeling of lattice structures by homogenization. Adv. Eng. Softw. **29**(7), 699–705 (1998)
27. Boutin, C., dell'Isola, F., Giorgio, I., Placidi, L.: Linear pantographic sheets: asymptotic micro-macro models identification. Math. Mech. Complex Syst. **5**(2), 127–162 (2017)
28. dell'Isola, F., Eremeyev, V.A., Porubov, A.: Advances in Mechanics of Microstructured Media and Structures, vol. 87. Springer, Berlin (2018)
29. Di Nino, S., Luongo, A.: A simple homogenized orthotropic model for in-plane analysis of regular masonry walls. Int. J. Solids Struct. **167**, 156–169 (2019)
30. De Angelo, M., Placidi, L., Nejadsadeghi, N., Misra, A.: Non-standard Timoshenko beam model for chiral metamaterial: identification of stiffness parameters. Mech. Res. Commun. **103**, 103462 (2020)
31. D'Annibale, F., Ferretti, M., Luongo, A.: Shear-shear-torsional homogenous beam models for nonlinear periodic beam-like structures. Eng. Struct. **184**, 115–133 (2019)
32. Antman, S.S.: The theory of rods. In: Linear Theories of Elasticity and Thermoelasticity, pp. 641–703. Springer (1973)
33. Antman, S.S.: Nonlinear Problems of Elasticity. Springer, Berlin (2005)
34. Capriz, G.: A contribution to the theory of rods. Riv. Mat. Univ. Parma **7**(4), 489–506 (1981)
35. Altenbach, H., Bîrsan, M., Eremeyev, V.A.: Cosserat-type rods. In: Generalized Continua from the Theory to Engineering Applications, pp. 179–248. Springer (2013)
36. Steigmann, D.J., Faulkner, M.G.: Variational theory for spatial rods. J. Elast. **33**(1), 1–26 (1993)